FACULTY OF SCIENCE
UNIVERSITY OF COPENHAGEN

Bachelor Thesis

The tropical Atlantic near-inertial velocity from Eulerian observations at moored measurement stations

Vega Theil Carstensen

Niels Bohr Institute
University of Copenhagen

June 12, 2013

Supervisor
Markus Jochum
Climate and Geophysics
Niels Bohr Institute
University of Copenhagen

Contents

1 Introduction **2**
1.1 Near-inertial waves . . . 2
1.2 Aim of study . . . 4

2 Data **5**
2.1 Moorings . . . 5
2.2 Current time series . . . 5

3 Time series analysis **6**
3.1 The near-inertial frequency band . . . 6
3.2 Spectral analysis . . . 7
3.2.1 The Fourier transform . . . 7
3.2.2 The near-inertial variance . . . 8
3.3 Filtering . . . 9
3.4 Comparison of the two methods . . . 10

4 Wind forcing **11**
4.1 Wind time series . . . 12
4.2 Near-inertial events at 4N . . . 13
4.3 Near-inertial events at 12N . . . 17

5 Decay rates of near-inertial waves **19**

6 The effect of sampling intervals **19**

7 Discussion **20**

8 Conclusion **21**

Bibliography **I**

A Mathematical description of the coriolis parameter **II**
A.1 Zonal velocity component . . . II
A.2 Meridional velocity component . . . III

List of Tables **IV**

List of Figures **IV**

Abstract

Near-inertial waves (NIWs) affect the depth and temperature of the mixed layer and thereby the energy transfer to the oceans. A discrepancy in the near-inertial (NI) velocity between coupled climate model and drifter buoy studies has lead to a parameterisation in the coupled climate model CCSM4 (Community Climate System Model version 4) which enhances the near-inertial velocity at midlatitudes in order to fit observations. NI velocities from drifter buoy studies are however quite uncertain due to interpolation methods, so in order to increase precision of the parameterisation of NIWs, it is necessary to investigate the NI velocity at fixed positions. This study has data from two tropical Atlantic moorings at 23W, 4N and 12N respectively. Two methods are used to obtain the near-inertial speed at the two locations in the tropical Atlantic Ocean. The first method determines the variance of the NI spectral band as the integral of the spectrum of the current time series in the limits of the band. The NI variance (the near-inertial kinetic energy) leads to NI velocities of 12.8 cm/s and 16.6 cm/s at 4N and 12N respectively. The second method filters the current time series using a Butterworth bandpass filter in the near-inertial frequency band ($0.7 - 1.3f_{\mathrm{I}}$, where f_{I} is the local inertial frequency). With the NI velocity defined as the mean of the NI current speed, the NI velocities are 9.6 cm/s and 12.9 cm/s at 4N and 12N respectively. Both methods suggest a general overestimation of the near-inertial velocities in recent drifter buoy studies.

Resumé

Nær-inertielle bølger påvirker dybden og temperaturen af blandingslaget og dermed energioverførslen til havet. En uoverensstemmelse i den nær-inertielle hastighed mellem en koblet klimamodel og drive-bøje studier har ført til en parameterisering i den koblede klimamodel CCSM4 (Community Climate System Model version 4), som øger den nær-inertielle hastighed på mellembreddegrader for at tilpasse modellen til observationerne. Nær-inertielle hastigheder fra drive-bøje studier er dog ganske usikre på grund af interpolationssmetoder, så for at øge præcisionen af parametriseringen af bølgernes hastighed i modellen er det nødvendigt at undersøge den nær-inertielle hastighed på faste positioner til sammenligning. Denne undersøgelse har strømhastighedsdata fra to tropiske atlantiske forankrede bøjer på 23°V, henholdsvis 4°N og 12°N. To metoder anvendes til at bestemme den nær-inertielle hastighed på de to steder i det tropiske atlanterhav. Den første metode bestemmer variansen af det nær-inertielle frekvensbånd som integralet af spektret af havstrømstidsserien. Den nær-inertielle varians (den nær-inertielle kinetiske energi) fører til nær-inertielle hastigheder på henholdsvis 12.8 cm/s og 16.6 cm/s ved 4N og 12N. Den anden metode filtrerer havsstrømstidsserien vha. et Butterworth båndpas filter i det nær-inertielle frekvensbånd ($0.7 - 1.3f_{\mathrm{I}}$, hvor f_{I} er den lokale inertielle frekvens). Med den nær-inertielle hastighed defineret som middelværdien af strømhastighed, fås nær-inertielle hastigheder på hhv. 9.6 cm/s og 12.9 cm/s ved 4N og 12N. Begge metoder tyder på en generel overvurdering af den nær-inertielle hastigheder i tidligere drive-bøje studier.

Abbreviations

CCSM4	Community Climate System Model version 4
CH08	Chaigneau et al. (2008), drifter buoy study
EL08	Elipot & Lumpkin (2008), drifter buoy study
FFT	Fast fourier transform
NH	Northern hemisphere
NI	Near inertial
NIW	Near inertial waves
SH	Southern hemisphere
SST	Sea surface temperature

1 Introduction

The world oceans have a crucial impact on the climate of the Earth. Climate models therefore include the oceans in atmospheric climate models to form a fully coupled climate model. Many different physical processes are included in these models, but not all of them are equally well understood. A recent attempt (Jochum et al., 2013) was made to improve the parameterisation of near-inertial waves (NIWs) in the Community Climate System Model version 4 (CCSM4). Wind stresses excite the ocean currents and near-inertial waves are the oceans' first response to this wind forcing. Near-inertial waves affect the deepening of the mixed layer and thereby the local sea surface temperature (SST), which can change the uptake of energy in the oceans.

The model exhibits the same patterns of near-inertial velocities as found through Lagrangian observations (e.g. Chaigneau et al. (2008)), however the predicted inertial velocities are too small at midlatitudes. This is accounted for in CCSM4 by amplifying the NI velocities at mid- to high latitudes and tapering off this amplification to zero at 5°. Between 15° and 5° the correlation between the bandpass filtered near-inertial velocity and the amplifying parametrisation breaks down due to this tapering off.

The observational studies are based on a large number of drifter buoys covering most of the world oceans. However, there are two major disadvantages of these studies. One is that the uncertainty of the computed near-inertial velocity is quite large (e.g. Elipot & Lumpkin (2008)) because of the gross methods used in interpolation and averaging. The other is that there are very few drifter buoys present in the tropics near the equator (10S-10N), because the currents are deflected by the Coriolis force, hence the drifter buoys are removed from the equatorial region.

The correlation between the modelled and parameterised near-inertial velocities decreases to zero near the equator, where the near-inertial frequency band merges with the energetic low-frequency band. However, the deep tropics is the site on Earth where the ocean is most sensitive to SST changes. Therefore, the uncertainty of the observed tropical near-inertial wave (NIW) energy must be reduced in order to improve the correction parameterisation of tropical near-inertial waves in the CCSM4. This should be done by means of analysis of near-inertial currents from tropical moorings, which may provide a more detailed picture of the subtropical to equatorial change in the near-inertial velocity.

1.1 Near-inertial waves

Inertial waves is the term for oscillations of a specific frequency in the interior of a rotating fluid. In the ocean, they arise from the movement of the ocean in the accelerated coordinate system of the Earth. The ocean is stirred up by winds and is pertubed from an equilibrium (level sea surface, no motion) and the restoring force of these waves is the Coriolis force.

Angular momentum is defined as $\vec{L} = \vec{R} \times \vec{V}$, where R is the distance to the axis of rotation and V is the velocity of the motion. Hence for a motion on the surface of the Earth

$$L = RV \sin\phi \tag{1.1}$$

where ϕ is the angle between $\vec{R}$ and $\vec{V}$. For a rigid body like the Earth, $V = R\omega$, where ω is the total rotation rate of the motion[1], $\phi = \pi/2$ for horizontal motions on the surface of the Earth and $V = V_{\text{motion}} + V_{\text{Earth}}$. This leads to an angular momentum of a horizontal motion on the surface of the Earth

$$L = R^2\omega \tag{1.2}$$

[1]Only the zonal component of the velocity of the motion contributes to the extra rotation rate of the motion.

where ω can be divided into two rotation rates: the rotation of the Earth itself (Ω) and the additional rotation rate due to the motion relative to the surface of the Earth (u/R),

$$\omega = \Omega + u/R \quad , \tag{1.3}$$

where u is the zonal velocity of the motion. The angular momentum must be conserved ($dL/dt = 0$) and thus a change in latitude (changing R, Ω is constant) will result in a change δu in the speed of the motion u,

$$R^2 \left(\Omega + \frac{u}{R}\right) = (R + \delta R)^2 \left(\Omega + \frac{u + \delta u}{R + \delta R}\right) \tag{1.4}$$

Since angular momentum is a zonal force, the zonal acceleration is

$$\frac{du}{dt} = 2\Omega v \sin\varphi + \frac{uv}{a} \tan\varphi$$

where a is the equatorial radius of the Earth and φ is the latitude ($R = a\cos\varphi$). The first term on the right is the Coriolis parameter ($f_{\mathrm{C}} = 2\Omega \sin\varphi$) arising from the accelerated coordinate system and the second term arises from the curvature of the Earth. At synoptic scale ($|u| \ll \Omega R \approx 70$ m/s) the curvature of the Earth is negligible, thus

$$\begin{aligned} \frac{du}{dt} &= 2\Omega v \sin\varphi \\ &= v f_{\mathrm{C}} \end{aligned} \tag{1.5}$$

where φ is the latitude. A similar differential equation can be obtained for the meridional velocity v (see Appendix A for a detailed derivation),

$$\begin{aligned} \frac{dv}{dt} &= -2\Omega u \sin\varphi \\ &= -u f_{\mathrm{C}} \quad . \end{aligned} \tag{1.6}$$

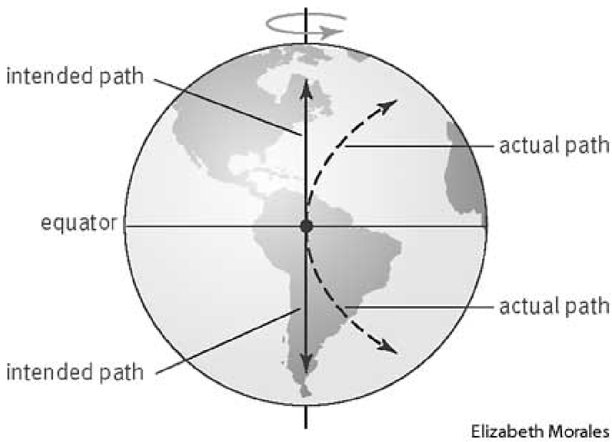

Figure 1.1: Schematic view of the deflection of motions by the Coriolis force. Motions rotate clockwise in the Northern Hemisphere (NH) and counter clockwise in the Southern Hemisphere (SH).

The magnitude of the Coriolis acceleration depends on the latitude φ. A water parcel in the Northern Hemisphere (NH) is always deflected to the right of the motion and will consequently rotate clockwise. Similarly a water parcel in the Southern Hemisphere (SH) is deflected to the left of the motion and will therefore rotate counter clockwise.

The further away from Equator the motion travels, the larger is the excess eastern velocity of the motion relative to that of the surface of the Earth, and the larger will the deflection of the motion be. The characteristic frequency of inertial oscillations thus depends on the latitude. This is often referred to as the local inertial frequency and it is equal to the local Coriolis parameter,

$$f_{\mathrm{I}} = 2\Omega \sin \varphi \tag{1.7}$$

where $\Omega = 1$ cpd $\approx 10^{-5}$ Hz is the rotational frequency of the Earth and φ is the latitude.

Near-inertial waves (NIWs) is the term for inertial waves with frequencies close to the local inertial frequency $f \approx f_{\mathrm{I}}$. These are traditionally included in analyses of inertial waves in order to take into account the propagation of the waves from other latitudes and thus the differences in the inertial frequency.

1.2 Aim of study

This study investigates current velocities at 10 m depth at two different tropical moored measurement stations in the tropical Atlantic Ocean. The primary goal is to determine the velocity of the near-inertial waves (the near-inertial velocity) at the two locations and compare these to the results of drifter buoy studies by Chaigneau et al. (2008), Elipot & Lumpkin (2008) and Elipot et al. (2010).

A secondary goal is to relate the large near-inertial events in the ocean to wind events. In addition, the effect of sampling intervals will be investigated along with the temporal decay of the near-inertial velocity.

2 Data

Current velocities in the zonal and meridional directions are measured at two tropical moored measurement stations at 10 m depths in units of cm/s. Wind velocities in the same directions are measured 4 m above the sea surface in units of m/s.

2.1 Moorings

Previous studies have relied on extensive datasets from drifter buoys (e.g. Chaigneau et al. (2008)). Drifter buoys have a very large spatial coverage (except at and near the equator), but due to gross interpolation methods the uncertainties are rather large (Elipot & Lumpkin, 2008). This study will focus on Eulerian measurements from a few selected tropical moorings for comparison with drifter buoy studies.

Moorings are floating buoys anchored at the sea bed with subsurface censors on the anchor line. The current velocities are measured using an acoustic doppler current profiler[2] (ACDP). The measurement at a given time stamp is an average of 2-3 min with sampling frequency 1 Hz.

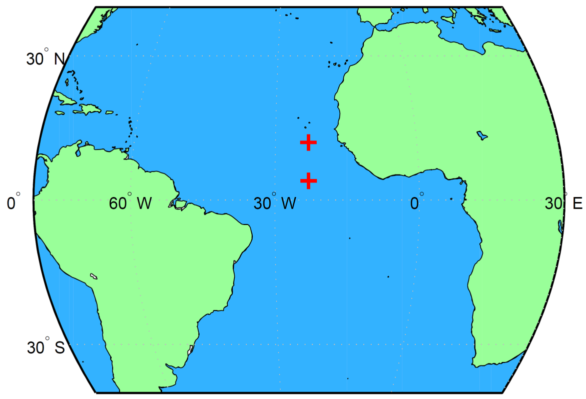

Figure 2.1: The tropical moorings are located at 4N 23W and 12N 23W (red plusses) in the tropical Atlantic Ocean. The measurements used in this study are those of zonal and meridional current velocities from 10 m depth and wind velocities from 4 m above the sea surface.

The two tropical moorings in the Atlantic are selected to be at different tropical latitudes, more specifically at 4N 23W and 12N 23W (see Figure 2.1). The temporal resolution of the current velocities at 4N and 12N is 20 min and 10 min respectively ($dt_{4\mathrm{N}} = 20$ min, $dt_{12\mathrm{N}} = 10$ min). The 4N time series starts on 11 May 2007 (19:40:00) and ends on 14 October 2008 (14:00:00); a time series of approximately 520 days with 72 measurements per day. The 12N time series starts on 8 June 2006 (15:00:00) and ends on 3 May 2007 (18:10:00); a time series of approximately 330 days with 144 measurements per day. The extracted time series is the longest possible continuous time span of simultaneous measurements in ocean currents and wind velocities at the given location.

Both time series include all four seasons, but there is no temporal overlap.

2.2 Current time series

The zonal and meridional current velocity time series from the two moorings are shown in Figure 2.2. The zonal velocities are shown in blue and the meridional are shown in red.

[2]The acoustic doppler current profiler uses the doppler shift of sound waves as means for determining the current velocity.

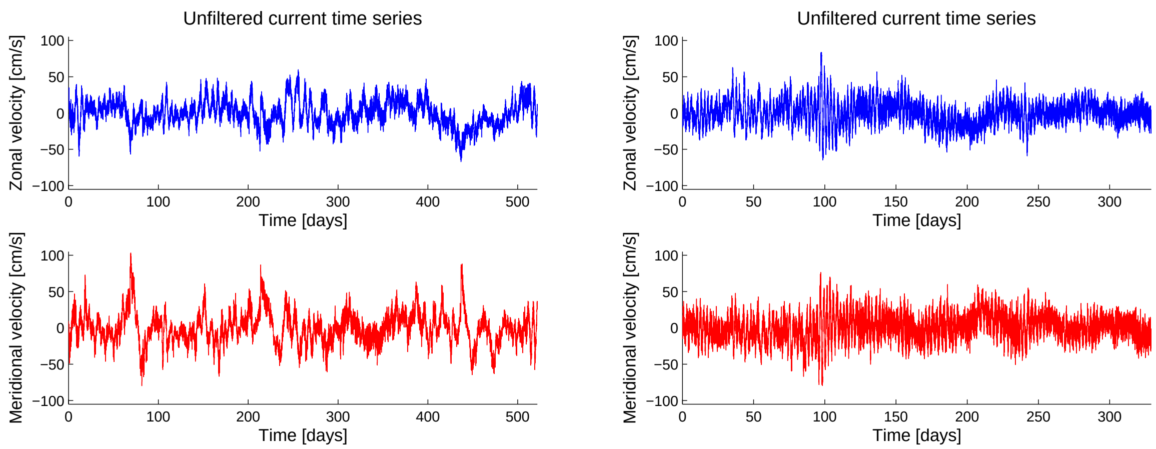

(a) 4N

(b) 12N

Figure 2.2: Original current velocity time series from two mooring locations. Zonal velocities are blue, meridional are red. Notice the higher temporal resolution and shorter temporal extent of the 12N time series.

Velocities are somewhat larger in the meridional direction at 4N with peak velocities up to 100 cm/s compared to the zonal peak velocities of approximately 60 cm/s. Velocities in the zonal and meridional direction at 12N are quite similar with peak velocities of 70-80 cm/s.

3 Time series analysis

Failed measurements are initially removed from the dataset (already done in Figure 2.2). NaN's occur between timesteps, indicating that they are artificially produced by an equipment error and they are left empty. Failed measurements (u_{cur} = -999 cm/s) are replaced by a mean of the two surrounding values in the dataset, a simple interpolation. Similarly the mean current in each direction is removed to avoid distortion of the near-inertial velocities.

3.1 The near-inertial frequency band

The original current time series contains ocean wave oscillations of many different frequencies, for example tidal waves with diurnal and semidiurnal frequencies. These frequencies are not the focus of this study. In order to estimate the near-inertial (NI) velocity it is necessary to isolate the frequencies of interest, namely the inertial frequencies of the two mooring locations (see Table 3.1).

Table 3.1: Inertial frequencies (1.7) and associated periods at the two mooring locations.

	Local inertial frequency f_{I}	Local inertial period T_{I}
4N	1.62 μHz or 0.14 cpd	7.14 days
12N	4.83 μHz or 0.42 cpd	2.40 days

The near-inertial frequency band is here defined as the band between $0.7f_{\mathrm{I}}$ and $1.3f_{\mathrm{I}}$ (Jochum et al., 2013), where f_{I} is the local inertial frequency. There are generally two ways of isolating the near-inertial frequency band.

One method is to do a spectral analysis and determine the strength of the NIWs from the relevant part of the frequency spectrum. This can be used for comparison with Lagrangian studies of the tropical NI variance (Elipot & Lumpkin (2008)). The extent to which this can be used as a measure for a NI velocity will be discussed later.

Another method is to filter the original time series with a suitable filter to remove oscillations with frequencies outside the NI band. This method is used to determine a typical near-inertial (NI) velocity for comparison with drifter studies (Chaigneau et al. (2008)) and model outputs (Jochum et al. (2013)) and the near-inertial velocity parameterisation in the CCSM4 can then be improved. The filtered time series can in addition be used to compare NI events with wind forcings.

3.2 Spectral analysis

The spectral analysis is used to determine the strength of the near-inertial band and thereby obtain the near-inertial variance for comparison with Elipot & Lumpkin (2008). The method chosen for the spectral analysis is the Fourier transform.

3.2.1 The Fourier transform

The fast Fourier transform (FFT) is used to quantify the strength of different frequencies in the current time series. The theory behind the method builds on the fact that any periodic discrete time series can be approximated by a discrete finite sum of sines and cosines

$$y(t) \approxeq \sum_{k}^{N/2} A_k \cos(\omega_k t) + B_k \sin(\omega_k t) \quad , \tag{3.1}$$

where $\omega_k = 2\pi k f_0$ is the k'th angular frequency, N is the length of the time series, $f_0 = 1/T$ is the fundamental frequency (the lowest detectable frequency of the time series) and T is the temporal length of the time series. The coefficients A_k and B_k are the amplitudes of the cosine and sine oscillations respectively with frequency ω_k and for a discrete time series of length N the coefficients are

$$\begin{aligned} A_k &= \frac{2}{N}\sum_{n=1}^{N} y_n \cos(2\pi kn/N), \quad k = 0, 1, 2, ..., N/2 \quad , \\ B_k &= \frac{2}{N}\sum_{n=1}^{N} y_n \sin(2\pi kn/N), \quad k = 1, 2, ..., N/2-1 \quad , \end{aligned} \tag{3.2}$$

where y_n is the discrete time series steps. The coefficients in (3.1) for frequencies $k > N/2$ are oscillations with frequencies higher than the maximum detectable frequency, the Nyquist frequency $f_{\mathrm{Nyq}} = 1/(2\Delta t) = f_0 N/2$. These will therefore if included wrongly contribute to lower frequencies, so-called undersampling.

The FFT results in a complex valued function of frequency ω_k

$$Z(\omega_k) = A_k + iB_k \quad . \tag{3.3}$$

The strength of the k'th frequency in the signal is $|Z(\omega_k)|^2 = A_k^2 + B_k^2$. Hereafter the frequency will be denoted f and will be considered to be continuous such that the frequency spectrum is defined as

$$|S(f)|^2 \propto \frac{|Z(f)|^2}{f_0} \quad , \tag{3.4}$$

where f_0 is the smallest frequency increment possible (= the fundamental frequency of the time series).

3.2.2 The near-inertial variance

The variance in the near-inertial band is

$$\sigma^2 = \int_{0.7f_{\mathrm{I}}}^{1.3f_{\mathrm{I}}} |S(f)|^2 df \tag{3.5}$$

(according to Parseval's theorem[3], this is also the variance of the filtered velocity time series) where $|S(f)|^2$ is the frequency spectrum and f_{I} is the local inertial frequency. For practical purposes the frequency spectrum is normalised such that the variance of a unit sine wave is one half, leading to a new definition

$$|S(f)|^2 = \frac{\sqrt{2}}{N}\frac{|Z(f)|^2}{f_0} \quad . \tag{3.6}$$

The frequency spectra of the zonal velocity components at 4N and 12N are shown in Figure 3.1. The local inertial frequency indicated is as a red line and the limits of the NI band $(0.7f_{\mathrm{I}} - 1.3f_{\mathrm{I}})$ are indicated as dotted lines. The near-inertial band is much more distinct from the rest of the frequency spectrum at 12N than at 4N, suggesting that a larger fraction of the energy is in the near-inertial band at this location. Two additional peaks stand out in both frequency spectra - the diurnal and the semidiurnal frequencies at 1 and 2 cpd respectively. Similar meridional spectra are not included here.

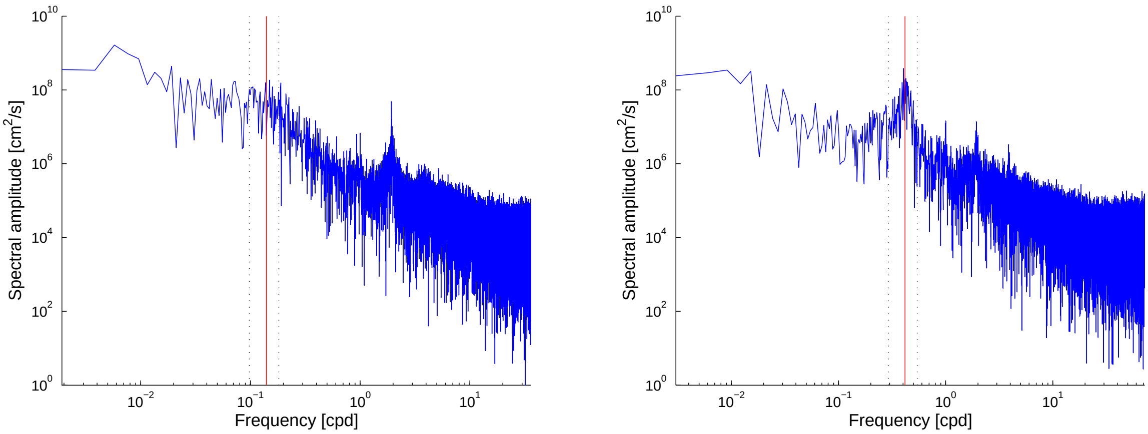

(a) 4N, zonal

(b) 12N, zonal

Figure 3.1: Frequency spectrum of (a) the 4N zonal time series and (b) the 12N zonal time series. The red line indicates the local inertial frequency and the dotted lines indicate the limits of the NI band. The energy contained in the near-inertial band is more distinct at 12N, while the semidiurnal frequency is stronger at 4N.

For the current time series $Z(f)$ has units of cm/s, resulting in a variance with units of kinetic energy ($\mathrm{m^2\,s^{-2}}$). Assuming that the variances are independent, the variances of the zonal and meridional directions can be added to give a variance for comparison with Elipot & Lumpkin (2008) and Elipot et al. (2010),

$$\sigma^2 = \sigma_u^2 + \sigma_v^2 \quad , \tag{3.7}$$

[3] Parseval's theorem states that $\int_{-\infty}^{\infty} |x(t)|^2 dt = \int_{-\infty}^{\infty} |X(f)|^2 df$; here $x(t)$ is the filtered time series and $X(f)$ is the frequency spectrum of the filtered time series (or to a good approximation the frequency spectrum of the original time series in the near-inertial band, hence $X(f) = S\,(f' \in [0.7f; 1.3f])$).

see Table 3.2. The NI variance determined by Elipot & Lumpkin (2008) is a basin average for, in this comparison, the Atlantic Ocean.

Table 3.2: NI variance calculated from the frequency spectrum in the local NI frequency band. The square brackets show the NI variance error bars of Elipot & Lumpkin (2008).

	σ^2_{EL08}	σ^2_{EL10}	σ^2_{NI}	
2.5N-5N	2.25 [1.00,6.50] $\cdot 10^{-2}$ m^2 s^{-2}	-	1.63 $\cdot 10^{-2}$ m^2 s^{-2}	4N 23W
10N-12.5N	1.90 [0.75,9.00] $\cdot 10^{-2}$ m^2 s^{-2}	2.51 $\cdot 10^{-2}$ m^2 s^{-2}	2.74 $\cdot 10^{-2}$ m^2 s^{-2}	12N 23W

3.3 Filtering

A bandpass filter is used to eliminate all frequencies outside the near-inertial frequency band. The current time series is filtered using a Butterworth bandpass filter in the NI band between $0.7 f_{\mathrm{I}}$ to $1.3 f_{\mathrm{I}}$.

The speed and direction of the NI current can be obtained from $\sqrt{u^2 + v^2}$ and $\theta = \tan^{-1}\left(\frac{v}{u}\right)$ and Figure 3.2 shows the direction of the NI currents at 4N and 12N respectively. The 4N NI current is slightly more often in the meridional direction, while at 12N it is equally often in all directions.

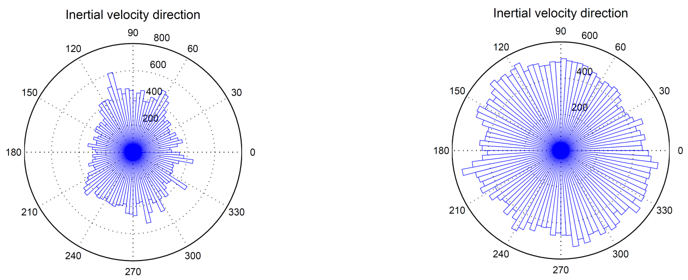

(a) 4N (b) 12N

Figure 3.2: Direction histograms of the NI current directions at the two mooring locations. The NI current directions are generally not polarised, however the 4N mooring exhibits a slightly preferred direction north-south, which could be attributed to the fact, that it is very close to equator, where currents are deflected away from the equator.

The filtered time series of the two moorings are plotted in Figure 3.3. The difference in the local inertial frequency at the two moorings is clearly visible from the filtered time series as the 12N time series oscillates at a higher frequency than the 4N time series. The currents are phase shifted with the zonal current velocity lagging about half a day (depending on latitude) after the meridional current. This initially confirms the inertial rotation of the current vector.

The nature of the filtered time series at 4N is very much different from the unfiltered time series (see Figure 2.2a, note the different scaling of the axes). The peak NI velocities are smaller than the broadband velocities and the large events appear at different times in the two time series. The 4N filtered time series shows a lot of variability in the near-inertial velocity. The filtered time series of the 12N mooring is more similar to the unfiltered time series, suggesting that the NIWs are responsible for much of the ocean kinetic energy at this latitude, which was already suggested by the zonal frequency spectra in Section 3.2.

The NI velocity time series at the two mooring generally exhibit inertial velocities of roughly the same size. However, the 12N time series shows more distinct events of NI velocities. The two directions

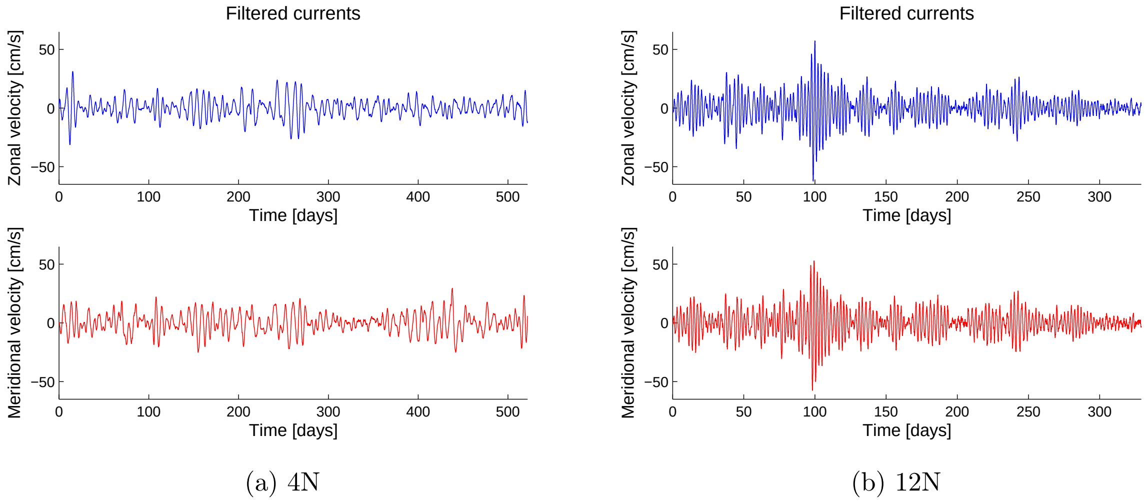

Figure 3.3: Filtered time series from the (a) 4N and (b) 12N mooring. The 12N time series generally show larger NI velocities than the 4N time series. The 12N time series shows more distinct near-inertial velocity events than the 4N time series.

of the 12N time series are more similar to each other than the two directions of the 4N time series. One peak stands out in the near-inertial velocity of the 12N time series.

The speed of the NIWs is calculated from the near-inertial velocity time series,

$$|\vec{U}_{\mathrm{NI}}| = \sqrt{u_{\mathrm{NI}}^2 + v_{\mathrm{NI}}^2} \quad , \tag{3.8}$$

and the mean of the resulting time series is then a measure of a typical near-inertial velocity at the given position. The near-inertial velocities at the two mooring locations are

$$\begin{aligned} U_{\mathrm{NI,4N}} &= 9.8 \text{ cm/s} \\ U_{\mathrm{NI,12N}} &= 12.8 \text{ cm/s} \end{aligned} \tag{3.9}$$

The NI velocity at 12N is larger than at 4N. Histograms of the NI velocity time series at the two positions are shown in Figure 3.4 with the mean NI velocity marked as a red line.

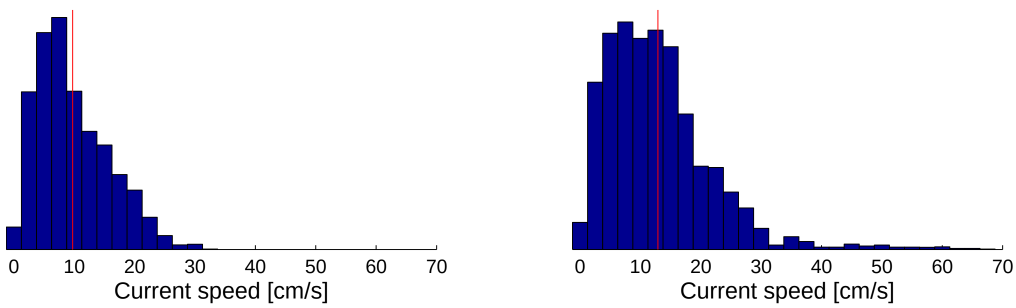

Figure 3.4: Near-inertial velocity histograms at the two mooring locations (4N left, 12N right) with mean NI velocity shown as a red line.

3.4 Comparison of the two methods

The NI variance is equal to the kinetic energy in the NI band (Elipot et al., 2010), thus a typical velocity of the NIWs can be obtained from this variance as well as by means of filtration.

The spectrum of the zonal filtered time series at 12N is shown in Figure 3.5 for comparison with the spectra of the unfiltered time series (see Figure 3.1b). The broadband variance of the filtered time series can be shown to be mathematically equal to the mean squared speed of the filtered time series,

$$\sigma_{\text{filt,broadband}} = \sqrt{\text{mean}\left(u_{\text{filt}}^2 + v_{\text{filt}}^2\right)} \quad . \tag{3.10}$$

This is somewhat larger than the method used by Jochum et al. (2013), where

$$U_{\text{NI}} = \text{mean}\left(\sqrt{u_{\text{filt}}^2 + v_{\text{filt}}^2}\right) \quad , \tag{3.11}$$

and somewhat smaller than the velocity from the NI variance of the original time series due to the slightly damped spectral amplitude in the edges of the NI band.

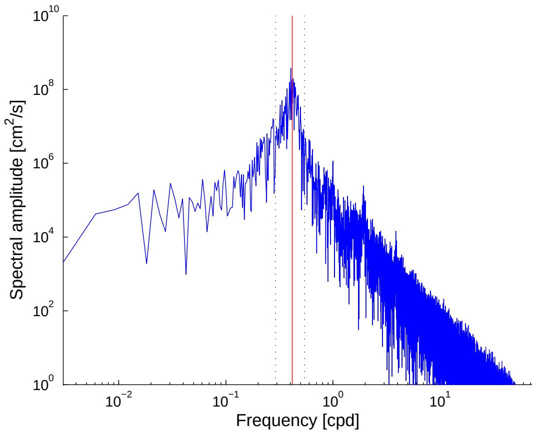

Figure 3.5: Zonal spectrum of the filtered time series at 12N.

Table 3.3: Components of the NI velocity calculated from the frequency spectra in the local NI frequency band and from the filtered time series.

	σ_{NI} (Table 3.2)	$\sigma_{\text{filt,broadband}}$ (eq. 3.10)	U_{NI} (eq. 3.11)
4N	12.8 cm/s	11.4 cm/s	9.8 cm/s
12N	16.5 cm/s	15.7 cm/s	12.9 cm/s

For comparison, the near-inertial velocities of the two methods are shown in Table 3.3, and it shows that the NI velocity from the spectrum is larger than that from the filtered time series as expected.

4 Wind forcing

The winds excite the ocean currents and therefore the winds are of great interest when examining the timing and magnitude of the NIWs. The winds are measured 4 m above the sea surface in units of m/s, and both moorings have a temporal resolution of the wind velocities of 10 min ($dt_{\text{wind}} = 10$ min).

4.1 Wind time series

The wind velocity is measured in the zonal and meridional directions, like the current time series. Failed measurements (u_{wind} = -99 m/s) are replaced by zeros as the wind is only used for visual comparison with the NI current time series. Figure 4.1 shows the directions of the wind vectors of the entire time series. The wind at 4N predominantly blows towards the north north-west, while the wind at 12N predominantly blows towards the south south-west.

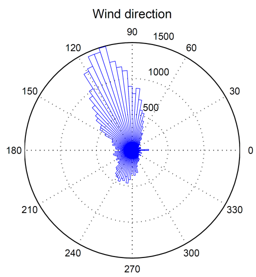

(a) 4N

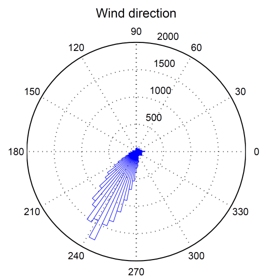

(b) 12N

Figure 4.1: Direction histograms of the wind velocity. The wind direction at 4N is mostly north north-west (NNW), and the wind direction at 12N is mostly south south-west (SSW).

The wind stress

$$\tau = c_d |\vec{U}_{\text{w}}|^2 \quad , \tag{4.1}$$

where $c_d = 1.3e^{-3} \approxeq 0.06$ is the dimensionless drag coefficient of the wind on the ocean and $\vec{U}_{\text{w}}$ is the wind speed vector, can be used to compare the magnitude of different events in the wind to assess their relative importance in exciting NI ocean currents.

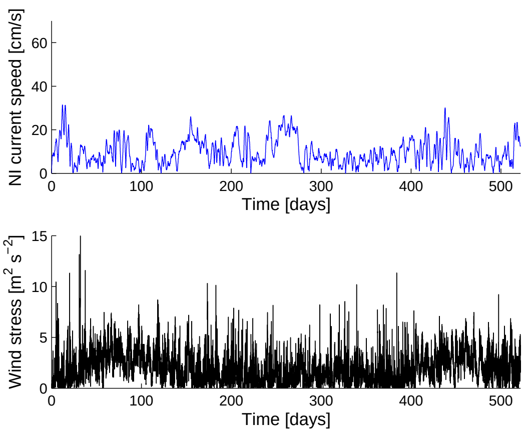

(a) 4N

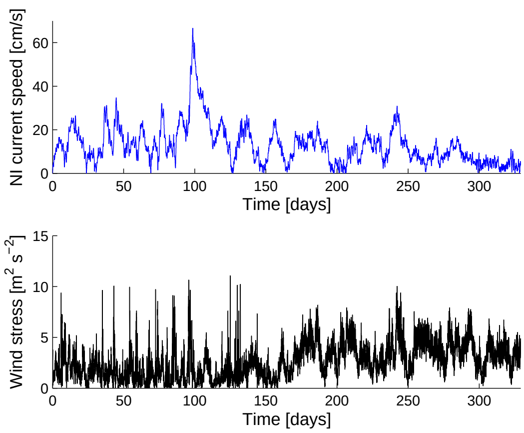

(b) 12N

Figure 4.2: Near-inertial speed time series and wind stresses at the two mooring positions. The wind stress at 12N has many peaks of order 10 m^2 s^{-2}, while the wind stress at 4N is generally smaller but with one apparent peak of 13 m^2 s^{-2} in the beginning of the time series.

The wind stresses and the NI current speed at 4N and 12N respectively are plotted in Figure 4.2. Comparing the speed time series of the two moorings, the currents are somewhat stronger at 12N than at 4N. The 12N wind stress has many peaks of order 10 m^2 s^{-2}, while the 4N wind stress is generally smaller, but with single peaks above 10 m^2 s^{-2}. However, the wind stress at the time of the large event in the NI speed at 12N is not significantly larger than for the rest of the time series, indicating that the wind stress is not the driving force for exciting NIWs. Similarly the largest current speed events at 4N does not seem to coincide with large wind stresses.

Dohan & Davis (2011) examined two consequent storm events of similar magnitude, but very different responses. They suggested that a resonant turning of the winds matching the local inertial frequency of the ocean has a large effect on the resulting magnitude of the inertial velocity.

In the next section, refocusing on the filtered current velocities (Figure 3.3) there are several distinct events that could have been caused by the wind. The timing of these events are compared to the wind time series in terms of both the wind stress and the resonant turning of the winds. Several distinct events are examined in the 4N time series, while in the 12N time series the focus is primarily with the one large event in the near-inertial velocity occuring around day 100 (September 2006).

4.2 Near-inertial events at 4N

In the zonal and meridional directions five peak NI velocity events at 4N are identified from Figure 3.3a. Excerpts of the time series around the time of the peaks are then compared to the wind velocities and directions.

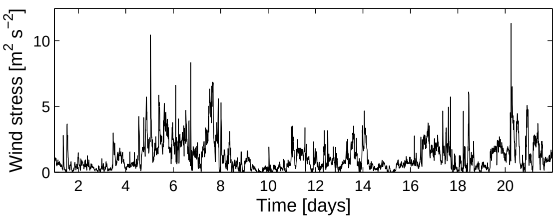

(a)

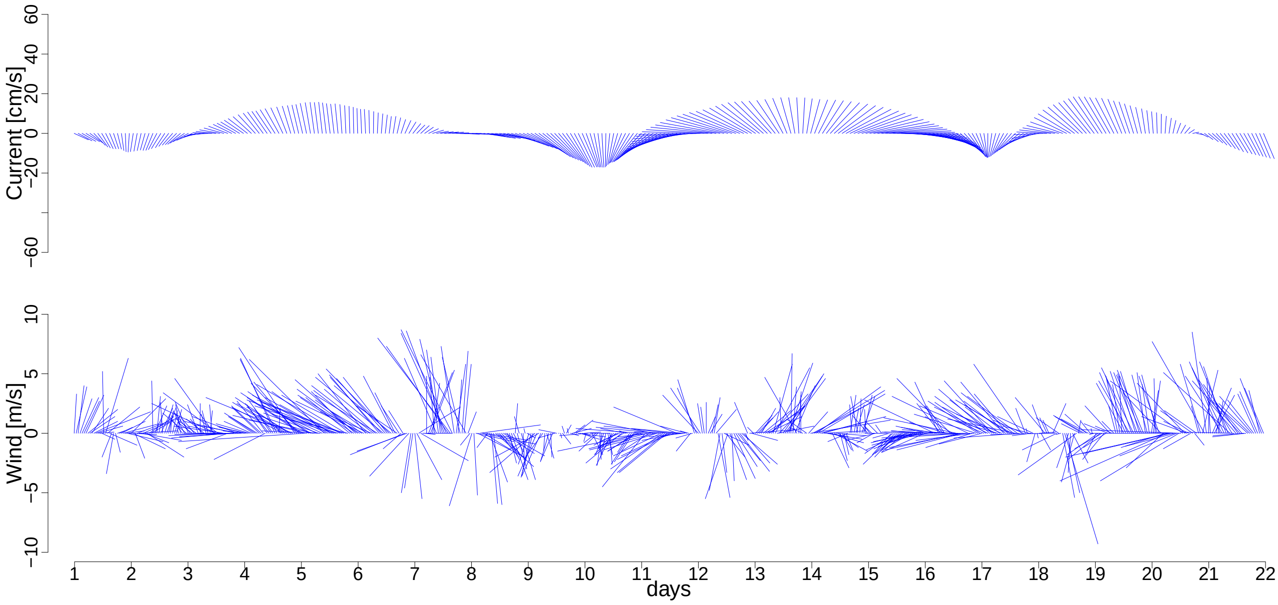

(b)

Figure 4.3: **days 1-22.** The wind stress is largest at days 5 and 20, which does not coincide with the largest excitation of NI currents, indicating that this is not the driving force of the NI currents of this period. Resonant turning of the winds at days 10-13 seem to excite NI currents.

4N event at days 1-22 The wind stress (Figure 4.3a) is largest around days 5 and 20, which does not coincide with the largest excitation of NI currents, indicating that the wind stress is not the driving force of the near-inertial waves at this time. A clockwise resonant turning of the wind vector seems to occur at days 10-13, which excites a near-inertial current, see Figure 4.3b.

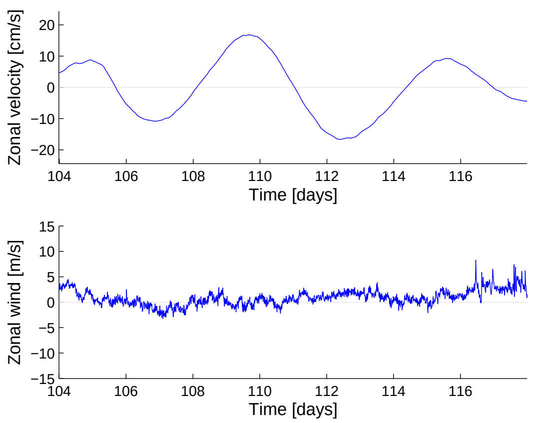

(a)

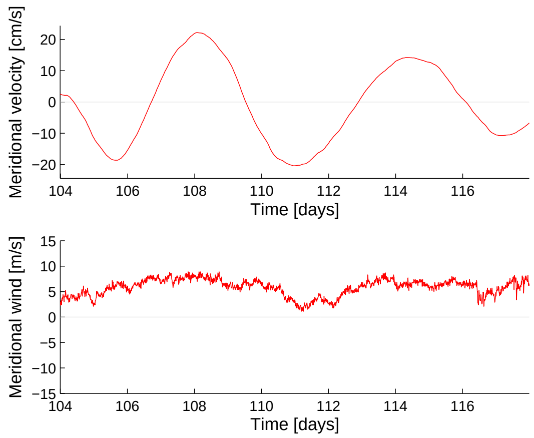

(b)

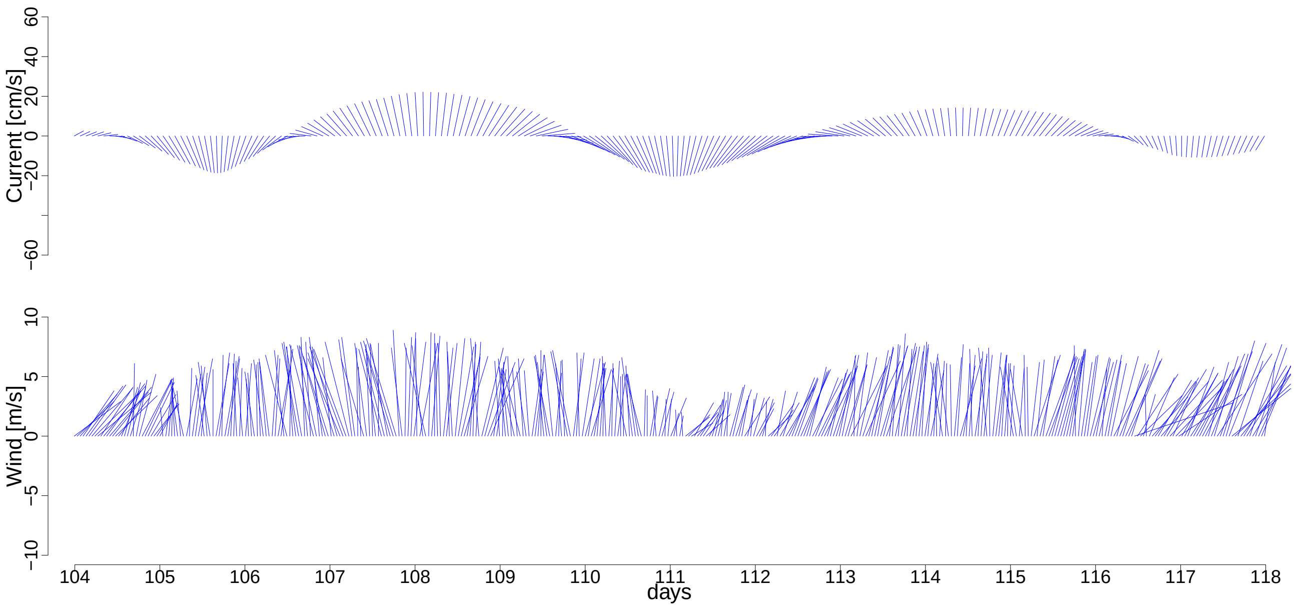

(c)

Figure 4.4: **days 104-118.** The wind velocities are generally small in this period. However, the periodicity of the meridional wind is similar to the excited near-inertial currents, suggesting that this may be the driving force in exciting the NI currents in this period. The inertial characteristics of the current are visible in both directions as it rotates clockwise (NH).

4N event at days 104-118 The event of large NI velocities at days 104-118 is a good example of the resonant behaviour of the ocean. The wind velocities are generally small (< 10 m/s), but the periodicity of the meridional wind speed nearly matches the inertial period at 4N. This results in large near-inertial velocities of $\mathcal{O}(20$ cm/s$)$. The reason for the large inertial currents in the zonal direction in the absence of a prominent zonal wind is a direct consequence of the fact that the current rotates, such that the velocities in the two directions are phase shifted.

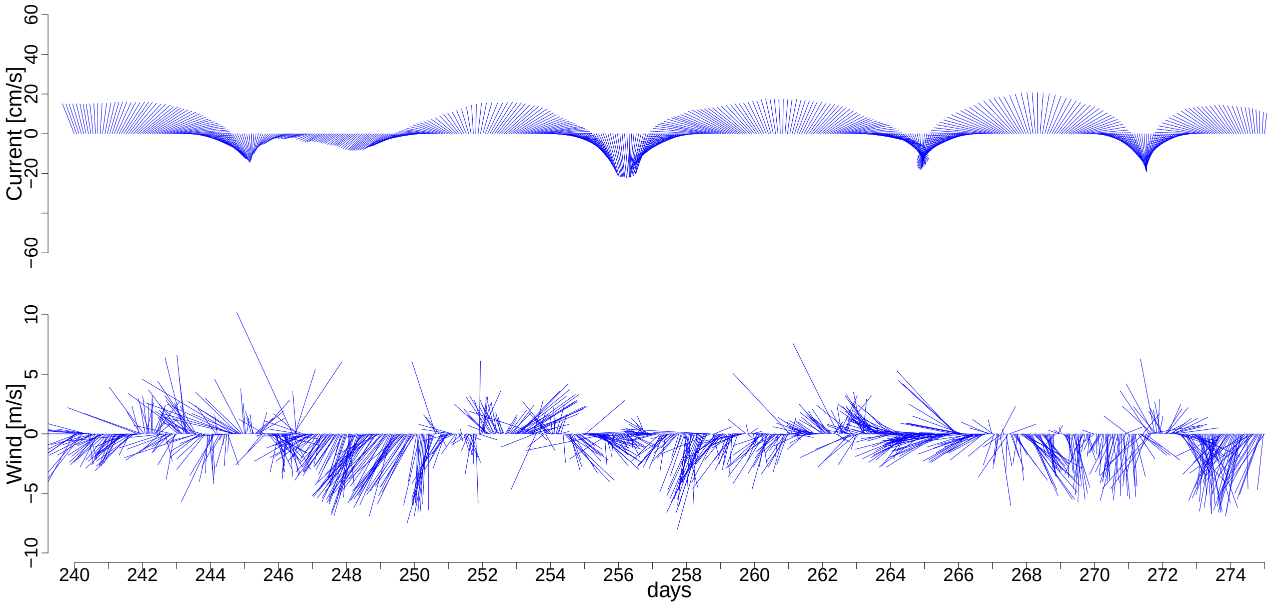

Figure 4.5: **days 240-275.** The winds turn with periods comparable to the local near-inertial frequency at days 245, 252-254 and 272. Near-inertial currents increase in magnitude and the inertially characteristic turning of the current is more prominent after these events.

4N event at days 240-275 The magnitude and inertial characteristics of the current are more prominent after the resonant turnings of the winds at days 245, 252-254 and 272. After around day 254 the truly inertial characteristic of the current is visible.

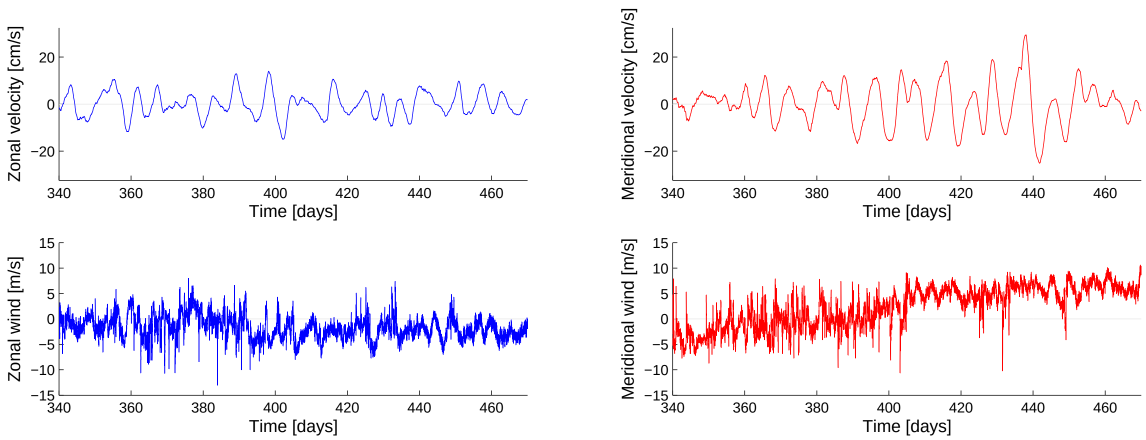

Figure 4.6: **days 340-470.** A steadily increase in the mean northbound wind velocity with short sudden southbound wind velocities excites meridional ocean currents. The zonal current velocities are however quite variable with no general trends, indicating that a true inertial current is never excited.

4N event at days 340-470 The steady increase in meridional wind velocity shown in Figure 4.6 induces an oscillating ocean current. However, the increase in the wind is not so significant that the current is truly inertial (or even near-inertial) and no near-inertial periodicity of the winds is visible as in Figure 4.4. The oscillating characteristics are not evident in both directions as would be expected for inertial currents, so this is an example of winds affecting the ocean current without an inertial response due to the lack of resonant turning in the winds.

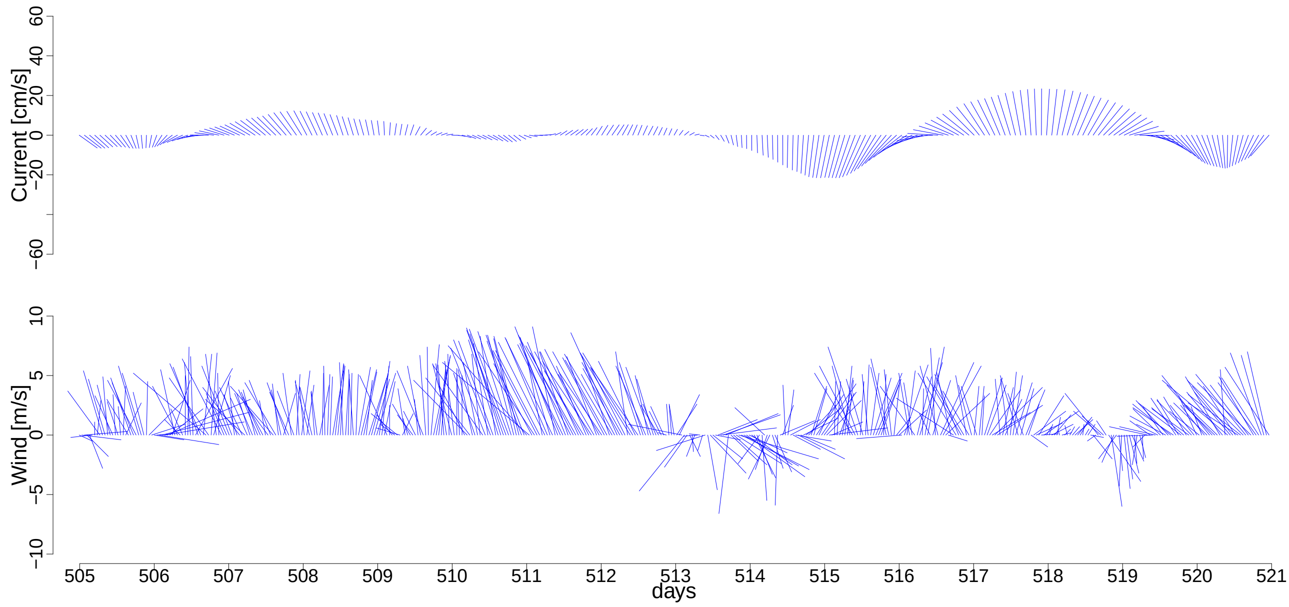

Figure 4.7: **days 505-521.** The winds generally blow towards north, which slows down the southbound current at day 510. At days 514-515 resonant turnings of the wind causes a large increase in the near-inertial speed. Several other resonant turnings in the winds at day 516-518 increases the inertial characteristics of the rotating current.

4N event at days 505-521 The meridional wind generally blow towards north, but a change in the winds at day 514 and especially a turning at day 517 induces NI currents in the ocean.

4.3 Near-inertial events at 12N

One large event in the 12N time series occurs from approximately September 2nd to October 11th 2006 (days 84-125) with the large peaks starting on the 12th of September (day 97). Most of the Atlantic tropical storms and hurricanes occur between June and November and in September 2006 the hurricane Helene formed in the proximity of the 12N mooring in the Atlantic Ocean, see Figure[4] 4.8.

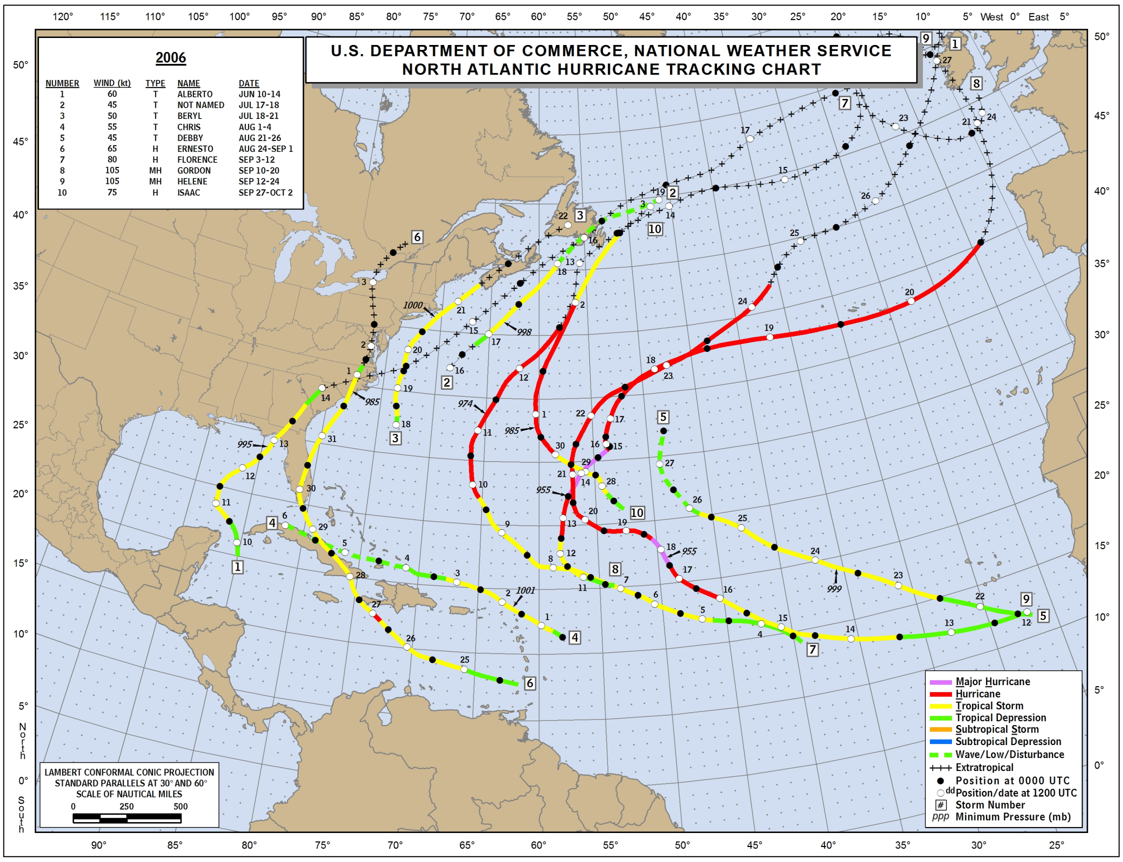

Figure 4.8: Track of hurricane Helene (September 2006) with date stamps and storm development. The green track (tropical depression) right around the 12N mooring at 12N 23W is the beginning of the tropical hurricane Helene. For reference, day 97 of the time series is September 12, 2006.

The wind stress of the period is comparable in size to wind stresses for the entire time series at 12N (see Figure 4.2b) and the wind velocities are only of $\mathcal{O}(10 \text{ m/s})$. This suggests that the fact that tropical hurricane Helene was in the proximity of the 12N mooring did not have a significant effect on the magnitude of the wind stress.

Instead the focus is directed towards the zonal and meridional wind time series of the period (days 93-107). Figure 4.9(a and b) shows the currents and winds in the period with these large NI current velocities, and Figure 4.9c shows the magnitude and directions of the currents and winds simultaneously.

[4]The illustration is borrowed from the National Hurricane Center (NHC) of the National Oceanic and Atmospheric Administration (NOAA), United States Department of Commerce; `http://www.nhc.noaa.gov/2006atlan.shtml`.

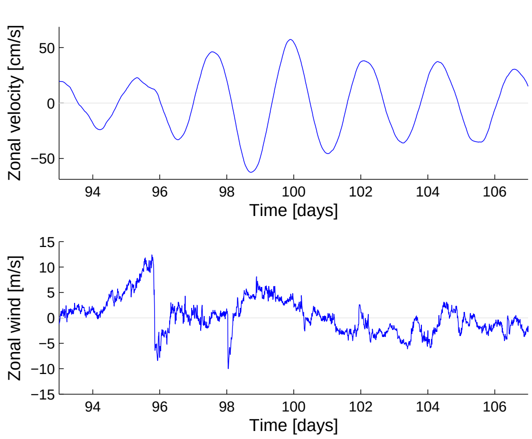

(a)

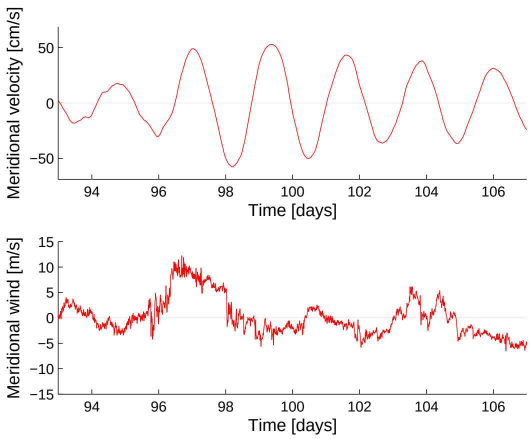

(b)

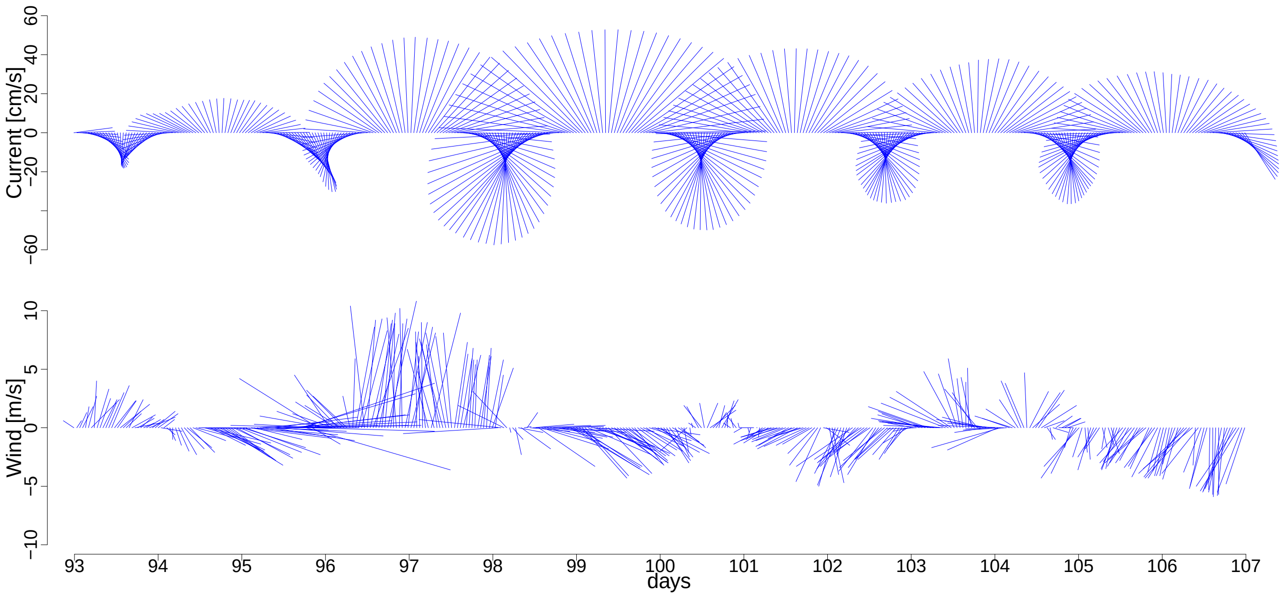

(c)

Figure 4.9: Wind and current time series for the period days 93-107 (September 10th-24th 2006) of the large near-inertial current event at the 12N mooring. The characteristic phase shift in the zonal and meridional near-inertial currents is visible, so is a large increase in the speed of the inertial currents with the characteristic inertial rotation after an inertial rotation of the winds at day 96.

A large meridional wind velocity at days 96-98 combined with a negative zonal wind velocity results in a turning of the winds with a period comparable to the local inertial frequency, see 4.9c. This is most clearly seen in the meridional wind at days 94-97 and in the meridional current at days 96-98 (slightly delayed). These two sections of the time series exhibit the same pattern of a rapid increase followed by somewhat of a stagnation and yet another rapid increase.

The resonant turning of the winds is most clearly seen around days 93 and 96. Especially at day 96 the wind vectors turn with a frequency close to the local inertial frequency and with larger wind speeds than at day 93. This results in an induced NI current with velocities up to 60 cm/s.

5 Decay rates of near-inertial waves

The near-inertial speed of three NI events in each of the two current time series are fitted with an exponential decay. The decay time τ of the NI speed (at which e^{-1} is left) is $\tau_{4\mathrm{N}} = 4.7 \pm 0.3$ and $\tau_{12\mathrm{N}} = 11.2 \pm 0.4$ respectively for the two locations.

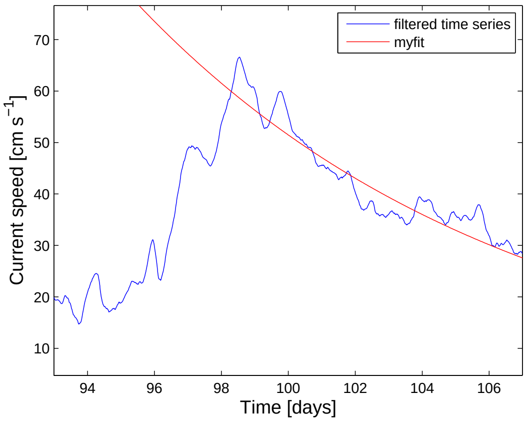

Figure 5.1: Example of exponential decay fit to the NI speed time series. The 12N mooring time series is shown for the period of days 93-107, when there is a large peak in the NI speed. The exponential decay is fitted from the largest peak and onwards (in this case days 98.5-107).

6 The effect of sampling intervals

The CCSM4 has a sampling frequency of 2 h, 6-12 times less frequently than the observations used in this study. The impact of these "larger sampling intervals" is studied by extracting single samples for each 10 min/20 min/1 h/2 h of the time series to form a new undersampled time series. The extracted values should not be a mean of the surrounding values, as this would obscure the difference in the data sought in order to asses the impact of the long sampling interval. The calculated NI velocities for the different time steps are listed in Table 6.1 as outputs from both methods.

Table 6.1: The changes in the computed near-inertial speed caused by changes in timestepping are shown for each timestep. Recall the temporal resolution of the 4N mooring ($dt_{4\mathrm{N}} = 20$ min).

	Filtration [cm/s]		**Spectrum [cm/s]**	
Timestep	**4N**	**12N**	**4N**	**12N**
10 min	*N/A*	12.9217	*N/A*	16.5436
20 min	9.7524	12.9529	12.7874	16.5674
1 h	9.7728	12.9349	12.8161	16.5422
2 h	9.8101	13.0177	12.8731	16.6393

As long as the sampling frequency is high enough that the inertial frequency can be resolved ($f_{\mathrm{sampling}} > f_{\mathrm{inertial}}$) the effect of timestepping seems to be negligible as the differences in the near-inertial speed are smaller than the uncertainty of the measured ocean currents.

7 Discussion

Elipot & Lumpkin (2008) (hereafter EL08) divided the drifters into zonal bands of 2.5° width in each basin (Pacific, Atlantic and Indian Oceans, north and south separately). Figure 3 of EL08 shows the zonally averaged drifter velocity variance σ^2 obtained from integration of the time series spectra in the interval from 0.9 times the minimum inertial frequency of the band to 1.1 time the maximum inertial frequency of the band. Elipot et al. (2010) (hereafter EL10) included a more detailed picture (1°×1° grid) of the NI variance (figure 9) of the same dataset. For comparison with this study the results of EL08 are used for the 4N position (see Table 3.2) since the results of EL10 does not extend all the way to 4N.

The NI variance in this study is the spectral integral between $0.7 f_\mathrm{I}$ and $1.3 f_\mathrm{I}$. Due to the difference in the limits of the integral[5] the variance at the 4N mooring of this study is expected to be somewhat lower than for the 2.5°-5° zonal band of EL08, which is consistent with the results shown in Table 3.2. The NI variance at 12N is slightly larger in this study compared to Elipot et al. (2010). This might be due to the large event in the 12N time series, which could be a rare event even with the resonant turnings of the winds.

Figure 1b of Chaigneau et al. (2008) (hereafter CH08) shows the amplitude of the near-inertial velocity. Close to the 12N mooring the NI speed is slightly below 10 cm/s. In the 5S-5N latitude band the inertial characteristics are not considered, however an immediate estimate for the location of the 4N mooring could be an inertial velocity of almost 20 cm/s. The simulation (CH08 figure 1d) shows a general enhancement of the inertial velocities at the equator, which is attributtable to the merger of the near-inertial frequency band with the energetic low-frequency band (Chaigneau et al. (2008)).

Figure 1a of Jochum et al. (2013) shows the mean zonal NI velocity output from the CCSM4 in cm/s, indicating[6] near-inertial velocities of 11-13 cm/s at 4N and 7-10 cm/s at 12N. Figure 1b of Jochum et al. (2013) shows the correlation between the modelled and corrected NI velocity. The correlation is quite low (0.1-0.3) near the equator, where the correctional parametrisation tapers off. The 4N mooring however lies in a pool of larger correlation (0.3-0.5), suggesting that the NI velocity at this location is well matched even without the tapered-off parameterisation developed to account for the discrepancies in the mid-latitude NI velocity field.

The near-inertial velocity of Jochum et al. (2013) is calculated directly from the filtered time series, whereas Elipot & Lumpkin (2008) (and Elipot et al. (2010)) calculated the NI velocity as the square root of the NI variance, which is equal to the kinetic energy of the near-inertial peak. This latter quantity is however always larger than the directly computed mean near-inertial speed except for in the case of a monochromatic oscillation of constant speed, as explained in Section 3.4.

[5] Elipot & Lumpkin (2008) integrates with limits $[0.91; 2.23] \times 10^{-6}$ Hz for the 2.5-5 degrees zonal band, while variance at 4N is calculated between limits $[1.13; 2.10] \times 10^{-6}$ Hz.

[6] Assuming that the NI velocities of the two directions are approximately equal, the NI velocity is a factor of $\sqrt{2}$ larger than the zonal NI velocity.

8 Conclusion

Recent drifter buoy studies suggest a larger near-inertial velocity at 4N than at 12N, as does the CCSM4. This is the reverse relationship between the near-inertial velocities at the two mooring positions relative to this study. This could be attributable to the large 12N event, which may be rare even with resonant turning of the winds resulting in a larger NI velocity at this location.

However, the near-inertial velocities still seem to be overestimated in drifter buoy studies, and an assesment of the discrepancy between the near-inertial velocities of the two methods used in this study should be studied perhaps with the use of statistical methods to improve comparison across studies and methods.

Acknowledgements

The moorings are fabricated and operated by the National Oceanic and Atmospheric Administration (NOAA). Data is available online with courtesy of the NOAA / PMEL / TAO Project Office, Dr. Michael J. McPhaden, Director.

Bibliography

Brown, Daniel P.: Tropical Cyclone Report, Hurricane Helene (AL092006), 12-24 September 2006. *National Hurricane Center*, `http://www.nhc.noaa.gov/2006atlan.shtml` (May 12, 2013)

Chaigneau, A., O. Pizzaro, and W. Rojas (2008): Global climatology of near-inertial current characteristics from Lagrangian observations. *Geophys. Res. Lett.*, **35**, L13603, doi: 10.1029/2008GL034060.

Dohan, Kathleen and Russ E. Davis (2011): Mixing in the transition layer during two storm events. *J. Phys. Oceanogr.*, **41**, 42-66, doi: 10.1175/2010JPO4253.1

Elipot, S. and R. Lumpkin (2008): Spectral description of oceanic near-surface variability. *Geophys. Res. Lett.*, **35**, L05606, doi: 10.1029/2007GL032874.

Elipot, S., R. Lumpkin and G. Prieto (2010): Modification of inertial oscillations by the mesoscale eddy field. *J. Geophys. Res.*, **115**, C09010 doi: 10.1029/2009JC005679.

Holton, James R.: An introduction to dynamic meteorology, 4th Edition. *Elsevier Academic Press*, 2004.

Jochum, M., B. P. Briegleb, G. Danabasoglu, W. G. Large, N. J. Norton, S. R. Jayne, M. H. Alford and F. O. Bryan (2013): The impact of oceanic near-inertial waves on climate. *J. Climate*, **26**, 9, 2833-2844, doi: 10.1175/JCLI-D-12-00181.1.

Knauss, John A.: Introduction to physical oceanography, 2nd Edition. *Waveland Press, Inc.*, 2005.

Thompson, L. A., S. Hautala and K. Kelly: Inertial oscillations lecture notes, 2005. Provided by supervisor Markus Jochum.

Whitford, Dennis J., Mario E. C. Vieira and Jennifer K. Waters (2001): Teaching time-series analysis. I. Finite Fourier analysis of ocean waves. *Am. J. Phys.*, **69**, 4, 490-496, doi: 10.1119/1.1331300.

A Mathematical description of the coriolis parameter

A.1 Zonal velocity component

Angular momentum ($\bar{L} = \bar{R} \times \bar{v}$) for a motion on the surface of the Earth is

$$L = Rv \sin \phi \tag{A.1}$$

where R is the distance from the motion to the rotation axis, v is the velocity of the motion on the surface and ϕ is the angle between R and v. For a rigid body like the Earth $v = R\omega$, where ω is the total rotation rate of the motion and $\phi = \pi/2$. This leads to the angular momentum of a motion on the surface of the Earth

$$L = R^2 \omega \tag{A.2}$$

where ω consists of two rotation rates: the rotation of the Earth itself Ω and the additional rotation rate due to the motion relative to the surface of the Earth u/R,

$$\omega = \Omega + u/R \quad . \tag{A.3}$$

The angular momentum must be conserved ($dL/dt = 0$) and thus a change in latitude (changing R) will result in a change in the speed of the motion u (Ω is constant).

$$R^2 \left(\Omega + \frac{u}{R} \right) = (R + \delta R)^2 \left(\Omega + \frac{u + \delta u}{R + \delta R} \right)$$
$$\delta u = -2\Omega \delta R - u \frac{\delta R}{R}$$

Dividing through by δt, taking the limit as $\delta t \to 0$ and remembering

$$\frac{\delta R}{\delta t} = \frac{\delta R}{\delta y} \frac{\delta y}{\delta t} = \frac{\delta R}{\delta y} v$$
$$\delta R = - \sin \varphi \delta y$$

the change in the zonal velocity is then

$$\frac{du}{dt} = 2\Omega v \sin \varphi + \frac{uv}{a} \tan \varphi \tag{A.4}$$

where a is the radius of the Earth and φ is the latitude ($R = a \cos \varphi$). The first term on the right is the Coriolis parameter f_C arising from the accelerated coordinate system that is the Earth and the second term arises from the curvature of the Earth. At synoptic scale ($|u| \ll \Omega R \approx 70$ m s^{-1}) the curvature of the Earth is negligible, thus

$$\begin{aligned} \frac{du}{dt} &= 2\Omega v \sin \varphi \\ &= v f_\mathrm{C} \end{aligned} \tag{A.5}$$

where φ is the latitude.

A.2 Meridional velocity component

A similar differential equation can be obtained for the meridional velocity v. The difference in the centrifugal force from a parcel at rest to a parcel moving due east is

$$\vec{F} = \frac{u_{\text{motion}}^2}{R}\hat{R} - \frac{u_{\text{rest}}^2}{R}\hat{R} \tag{A.6}$$

Using $u = \omega R$

$$\begin{aligned}\vec{F} &= \omega_{\text{motion}}^2 \vec{R} - \omega_{\text{rest}}^2 \vec{R} \\ &= \left(\Omega + \frac{u}{R}\right)^2 \vec{R} - \Omega^2 \vec{R} \\ &= \frac{2\Omega u}{R}\vec{R} - \frac{u^2}{R^2}\vec{R}\end{aligned} \tag{A.7}$$

The acceleration can then be divided into the vertical and meridional components using $R = a\cos\varphi$ and the trigonometric relations shown in the figure below,

$$\begin{aligned}\frac{dv}{dt} &= -2\Omega u \sin\varphi - \frac{u^2}{a}\tan\varphi \\ \frac{dw}{dt} &= 2\Omega u \cos\varphi + \frac{u^2}{a}\end{aligned} \tag{A.8}$$

As for the meridional velocity, at synoptic scale ($|u| \ll \Omega R \approx 70\ \mathrm{m\,s^{-1}}$) the curvature of the Earth is negligible, thus

$$\begin{aligned}\frac{dv}{dt} &= -2\Omega u \sin\varphi \\ \frac{dw}{dt} &= 2\Omega u \cos\varphi\end{aligned} \tag{A.9}$$

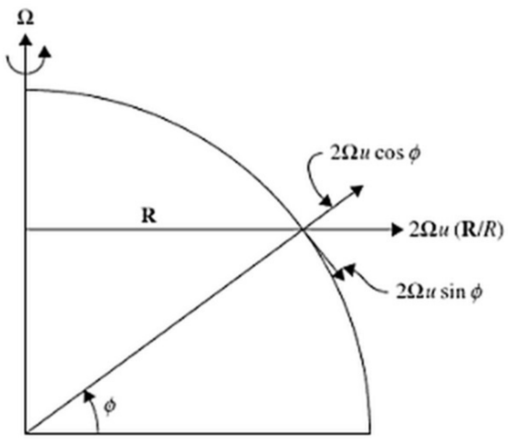

Figure A.1: Schematic view of forces arising from a change in the centrifugal force.

List of Tables

3.1 Inertial frequencies 6
3.2 Near inertial variance of the spectra 9
3.3 Near inertial speed 11
6.1 Impact of timestepping 19

List of Figures

1.1 Deflection by Coriolis force 3
2.1 Mooring positions 5
2.2 Original current time series 6
3.1 Zonal frequency spectra 8
3.2 Current roses 9
3.3 Filtered time series 10
3.4 Near-inertial velocity histograms 10
3.5 Spectrum of filtered zonal time series (12N) 11
4.1 Wind roses 12
4.2 Near inertial speed time series 12
4.3 4N event: days 1-22 13
4.4 4N event: days 104-118 14
4.5 4N event: days 240-275 15
4.6 4N event: days 340-470 15
4.7 4N event: days 505-521 16
4.8 Track of hurricane Helene 17
4.9 Large 12N event: days 93-107 (vectors) 18
5.1 Example of exponential decay 19
A.1 Meridional and vertical deflection by Coriolis force III